Communication

SAR Reduction With Antenna Cluster Technique

Harri Varheenmaa, Pasi Ylä-Oijala, Anu Lehtovuori, and Ville Viikari

Abstract—An efficient and straightforward antenna design method is presented that maximizes the ratio of total efficiency and specific absorption rate (SAR). This goal is achieved with a multiport antenna cluster technique where several ports are excited collectively with appropriate feeding weights. These weights are found as an eigenvalue solution formulated in terms of the radiated and near-field power of an antenna. The method relies on both the near-field (SAR) and far-field (radiation) physics of an antenna and it can be applied to various design cases. The importance of the maximization of total efficiency-SAR ratio and the feasibility of the proposed approach are demonstrated with a simple multiple-dipole antenna example and with a more realistic antenna design where a metal-rimmed antenna is held in the user's hand.

Index Terms—Antenna cluster, mobile antenna, Rayleigh quotient (RQ), specific absorption rate (SAR).

I. INTRODUCTION

The number of antennas used in close proximity to the user is continuously increasing emphasizing the importance of exposure-aware antenna design. Safety limits are determined with a parameter called the specific absorption rate (SAR). This parameter measures the absorbed electromagnetic power per unit mass of tissue. Both the American [1] and the European standards [2] have defined limits for maximum SAR values. These values have to be taken into account in the design of mobile devices [3], [4], [5], [6] as well as in different wearable antenna solutions [7], [8], [9].

Several detailed studies have been performed in the past to predict the SAR of an antenna (see, e.g., [10], [11]). In these studies, the focus is more on the estimation of the SAR than on reducing it. In addition, SAR computation is typically performed as a postprocessing step once the antenna has been designed [12], rather than taking SAR minimization as a design goal.

The easiest way to achieve the SAR safety limits is to lower the transmit power, but the reduction in transmit power leads to weaker transmitted fields and reduced coverage. Another straightforward way to reduce SAR is to locate antennas as far as possible from the user, for example, to the bottom of the device. This approach is not suitable for modern multiantenna mobile devices since all antennas cannot locate at the bottom of the device. Other widely used methods are insulating the antenna with wave-absorbing material, or shielding it with conductive material [13], [14], [15]. The downside of these methods is that they typically affect negatively the gain, efficiency, and bandwidth of the antenna [4]. Metamaterial structures [16], [17], [18] and electromagnetic bandgaps [19] have also been studied in SAR reduction. In practice, however, implementation of these structures into modern thin and small ground clearance devices is difficult due to their large size [3].

The previously presented methods for reducing SAR typically require additional materials or a sophisticated design of antenna structures. In addition, these methods may have a negative effect on the radiation properties of an antenna. In this communication, we introduce a novel and straightforward computational approach that can be applied to various design cases to optimize the performance of an antenna structure both in near and far-field to achieve the desired behavior from both the SAR and efficiency point of view. This is attained by utilizing an antenna cluster technique with collectively excited multiple feeding ports. The problem of finding optimal feeding weights is formulated as a Rayleigh quotient (RQ) and the optimal weights are found as a solution of a generalized eigenvalue equation. Eigenvalue formulations and RQs [20] have been previously used to solve optimal multiport feeding signals with various goals, such as maximization of impedance matching [21] or radiation efficiency [22]. To our knowledge, this is the first time when these approaches are utilized in SAR reduction.

To measure the performance of an antenna from both radiation and SAR point of view, we define a figure-of-merit (FoM)—the ratio of total efficiency and maximum SAR. Since this FoM cannot be formulated as an RQ, we need to define another quantity that models it as well as possible. To this end, we consider the ratio of radiated far-field power and surface near-field power. Since this ratio can be formulated as an RQ, it leads to a computationally extremely efficient method requiring the solution of an eigenvalue equation in which the dimension agrees with the number of ports. Another benefit of the method is that it relies on both the near-field and far-field physics of an antenna and thus is available in various design scenarios.

Numerical experiments with a simple multiple-dipole antenna are used to illustrate the importance of the choice of the optimization goal. We also show that solely optimizing standard antenna parameters such as total or radiation efficiency, or matching, may not produce an optimal solution from the SAR point of view. The feasibility of the proposed approach using the ratio of far-field and near-field powers as an optimization goal is demonstrated with a more realistic antenna example where a metal-rimmed mobile antenna is held in the user's hand.

II. SAR OPTIMIZATION

In the design and analysis of modern complicated antenna systems, it is seldom sufficient to study or optimize only a single design parameter, rather several factors have to be treated simultaneously. This is also the case with SAR optimization. The particular challenge with the minimization of SAR is that it easily leads to minimizing radiation and matching efficiency, too.

A. Definition of SAR and FoM

Let us consider a situation where a perfectly conducting lossless antenna is in close proximity to human tissue. The human tissue is modeled by a homogeneous, dispersive, and lossy dielectric object with complex permittivity.

SAR is defined as the power absorbed by the unit mass of tissue [23], [24]. The dielectric body is divided into small cubes D_i with mass m, and at a fixed time-harmonic frequency, so SAR is associated with the cube center point c_i as

$$\text{SAR}_i\,(c_i) = \frac{1}{2V_i} \int_{D_i} \frac{\sigma\,(r)\,\|E\,(r)\|^2}{\rho\,(r)}\,dV. \tag{1}$$

Here, V_i is the volume of D_i, σ and ρ are the conductivity and density of the tissue, respectively, and E is the electric field.

As mentioned above, it may not be sufficient to study solely SAR. Rather, for a realistic antenna, for example, a handset or wearable, both the total efficiency and SAR must be taken into account during the design process. We define an FoM that describes the ratio of the total efficiency, η_{tot}, and the maximum SAR

$$\text{FoM} = \xi\,\frac{\eta_{\text{tot}}}{\max\,(\text{SAR}_i)}, \quad \eta_{\text{tot}} = \frac{P_{\text{rad}}}{P_{\text{in}}}. \tag{2}$$

Here, P_{rad} and P_{in} are the radiated and input power of an antenna, and $\xi = P_{\text{in}}/m$ is a normalization factor. Mass m is either 1 or 10 g depending on the used SAR standard.

The benefit of the low SAR is that it enables higher input power without exceeding SAR safety limits. Naturally, higher input power means higher transferred power. Since the FoM takes into account both the SAR and the total efficiency, the antenna with a high FoM can transfer more power while the SAR value is still below the safety limits.

B. RQ and Near-Field Power

From the numerical optimization point of view, the definition of maximum SAR poses two challenges. First, SAR depends on the position, and the optimization process can be sensitive to the choice of the cube center c_i. Second, the definition of a cube where SAR is evaluated is rather complicated as the cube is near the surface of the body [25].

Our goal is to formulate the optimization problem as an RQ. The optimal solution to the problem can then be found by solving an eigenvalue problem

$$A\,x_n = \lambda_n\,B\,x_n \tag{3}$$

and time-consuming numerical optimization can be avoided. The wanted optimal solution is the eigenvector x_n corresponding to the maximum (or minimum) eigenvalue λ_n. Obviously, FoM defined in (2) cannot be expressed as an RQ. Therefore, we need to find another quantity that describes FoM as well as possible and can be expressed as an RQ.

In [23], it is demonstrated that the maximum electric field appears on the surface of the body block. This means that in minimizing maximum SAR, it is sufficient to study the maximum electric field on the body surface and minimize it. However, using a field value defined at a single point is usually numerically unstable and sensitive even to very small numerical errors. To avoid this problem, we consider the near-field surface power defined here as

$$P_{\text{near}} = \frac{1}{2\eta_0} \int_S \|E\,(r)\|^2\,dS \tag{4}$$

where the electric field is integrated over a surface S and $\eta_0 = \sqrt{\mu_0/\varepsilon_0}$ is the free space wave impedance.

The optimization goal is then formulated as the ratio of the radiated (far-field) power and the surface (near-field) power. In Section II-C, it is shown that this ratio can be expressed as an RQ in terms of port input currents.

C. Formulation With Port Input Currents

Let us next assume that the antenna structure includes P feeding ports and let $I = [I_1, \ldots, I_P]^T$ denote the complex-valued input currents of the ports. These port input currents are the unknowns to be optimized. First, the radiated power is expressed utilizing the far-field matrix F^{far} [26] with elements

$$F_{pq}^{\text{far}} = \frac{1}{\eta_0} \int_{S_\infty} E_p^*\,(r) \cdot E_q\,(r)\,dS, \quad p, q = 1, \ldots, P. \tag{5}$$

Here, S_∞ is a spherical surface in the far-field region, E_p is the electric field due to unit input current at port p, and $(\cdot)^*$ denotes complex conjugate. Using F^{far}, we have

$$P_{\text{rad}} = \frac{1}{2} I^H F^{\text{far}} I \tag{6}$$

where $(\cdot)^H$ denotes Hermitian transpose. Analogously, we define a near-field matrix with elements

$$F_{pq}^{\text{near}} = \frac{1}{\eta_0} \int_S E_p^*\,(r) \cdot E_q\,(r)\,dS, \quad p, q = 1, \ldots, P \tag{7}$$

and express the near-field surface power as

$$P_{\text{near}} = \frac{1}{2} I^H F^{\text{near}} I. \tag{8}$$

Obviously, both matrices F^{far} and F^{near} are positive definite, and the ratio of the far-field radiated power and the near-field surface power can be formulated as an RQ. Consequently, the generalized eigenvalue equation to be solved reads

$$F^{\text{far}} I_n = \lambda_n F^{\text{near}} I_n \tag{9}$$

and the optimal solution (port input currents) is the eigenvector I_n corresponding to the largest eigenvalue λ_n.

D. Numerical Implementation

The far-field and near-field matrices, needed in the eigenvalue equation (9), are implemented using an in-house MoM code for combined PEC and lossy dielectric bodies [27], [28] with multiple feeding ports. For given inputs, the program finds the equivalent electric surface current on the antenna and the equivalent electric and magnetic surface currents on the surface of the dielectric block. Matrices F^{near} and F^{far} are constructed by using unit inputs at the ports, one by one, and by computing the corresponding electric field in the near and far-field regions.

While the assembly of the far-field matrix requires numerical integration, the near-field matrix F^{near} can be obtained directly from the MoM solution. Let $J = n \times H$ and $M = -n \times E$ denote the equivalent electric and magnetic currents on the surface S of the dielectric body. The surface electric field at point $r \in S$ is given by

$$E\,(r) = n\,(r) \times M\,(r) - \frac{n\,(r)}{j\omega\varepsilon} \nabla_s \cdot J\,(r). \tag{10}$$

Here, $\nabla_s \cdot J$ is the surface divergence of J, and n is the exterior unit normal vector of S. In the numerical solution, integral (7) is evaluated at the center points of the triangles of the surface mesh and the integration weights are the areas of the triangles. Thus, the elements of the near-field matrix can be obtained as

$$F_{pq}^{\text{near}} \approx \frac{1}{\eta_0} \sum_{n=1}^N A_n E_p^*\,(r_n) \cdot E_q\,(r_n) \tag{11}$$

where A_n and r_n are the area and the center point of a triangle T_n on S, respectively. The electric field is evaluated using (10).

E. Other RQ-Based Optimization Goals

Above we showed how the ratio of far-field power and near-field power can be expressed as an RQ. To compare this approach with other design goals, next we shortly review the formulation of other antenna design parameters as RQs. Let S be the S-parameter matrix of a multiport antenna. Total active reflection coefficient (TARC), defined as

$$\text{TARC} = \sqrt{\frac{a^H \left(S^H S\right) a}{a^H a}} \quad (12)$$

can be formulated as an eigenvalue problem [20]

$$\lambda_n = \min \text{eig} \left(S^H S\right) \quad (13)$$

and the "TARC-optimal" solution is the eigenvector corresponding to the eigenvalue λ_n. Also radiation efficiency

$$\eta_{\text{rad}} = \frac{P_{\text{rad}}}{P_{\text{rad}} + P_{\text{diss}}} = \frac{I^H F^{\text{far}} I}{I^H R I} \quad (14)$$

and total efficiency

$$\eta_{\text{tot}} = \frac{P_{\text{rad}}}{P_{\text{in}}} = \frac{I^H F^{\text{far}} I}{a^H a} \quad (15)$$

can be formulated as RQs, since all involved matrices are Hermitian and positive definite. Here, $a = (Z_0)^{-1/2}(Z + Z_0)I$, with a diagonal matrix Z_0 including the characteristic impedances of the ports, and P_{diss} is the dissipated power due to dielectric losses. The dissipated power can be expressed with the real part of the port input impedance matrix, $Z = R + jX$, and the far-field matrix as

$$P_{\text{diss}} = \frac{1}{2} I^H \left(R - F^{\text{far}}\right) I. \quad (16)$$

If the antenna is lossy, radiation efficiency should include the contribution of metallic losses, too. In most practical situations, dielectric losses due to human tissue dominate over metallic losses and the assumption of a lossless antenna are reasonable.

III. EXAMPLES

In this section, we demonstrate the feasibility of the proposed method in maximizing FoM and investigate solutions with different input weight optimization goals. The first example considers a cluster of three dipole antennas on top of a dielectric (fat) block. The second one involves a more practical metal-rimmed mobile antenna device in a human hand. The optimal feeding weights for the multiport antenna are solved with in-house codes, and the corresponding SAR, S-parameter, and efficiency results are computed with CST Studio Suite.

A. Three Dipoles

The goal of this section is to compare different input weight optimization goals to show that traditional approaches may lead to prohibitively high SAR values. We consider a cluster of three dipoles of lengths (46, 48, and 50 mm) placed above a fat block of dimensions 40 mm × 72 mm × 30 mm. Due to the dissenting lengths of the dipoles, the resonance frequencies of the dipoles are different. This enables effective utilization of the antenna cluster technique and achieves wider bandwidth. The simulation setup is shown in Fig. 1. The distance between the dipoles is 11 mm, and the distance between the dipoles and the fat block is 5 mm. The size of the dielectric block is chosen large enough to model an antenna close to a human body so that edges do not have a significant effect on the results. In this example, the parameters of the fat block ($\varepsilon_r = 10.6$, $\delta = 0.389$ S/m, and $\rho = 911$ kg/m^3) are assumed frequency-independent.
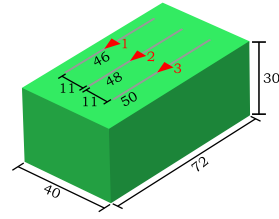

Fig. 1. Illustration of a three dipole cluster on top of a fat block. Dimensions are in mm. The distance between the dipoles and the block is 5 mm. Discrete ports, at the centers of the dipoles, are indicated with red arrows.
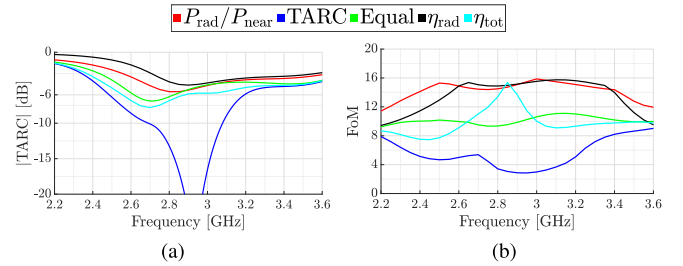

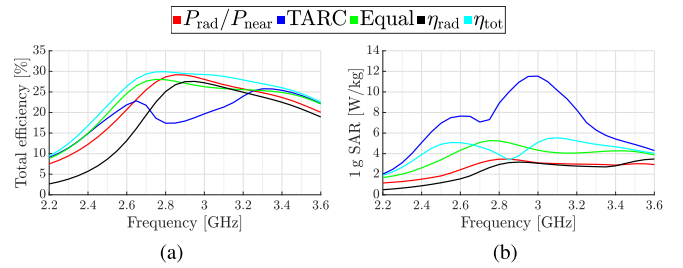Fig. 2. (a) TARC and (b) FoM of the three dipoles with different feeding weights.

Fig. 3. (a) Total efficiency and (b) maximum 1 g of SAR of the three dipoles with different feeding weights. The total input power is 22.4 dBm (175 mW).

The feeding weights of the dipoles are found by using four different optimization goals: TARC, η_{rad}, η_{tot}, and $P_{\text{rad}}/P_{\text{near}}$. The optimal solutions are based on the RQ formulations introduced in Sections II-C and II-E. In addition, we show results also for a nonoptimized case, that is, when all three dipoles have equal feeding weights (equal in legends).

Fig. 2(a) shows TARC with different feeding weights. Naturally, the TARC-optimized weights give the best TARC. Differences between other optimization goals are rather small but η_{tot} and equal weights lead to slightly better matching than $P_{\text{rad}}/P_{\text{near}}$ or η_{tot}.

The FoM, defined as in (2), with 1 g of SAR and with different excitation weights, is illustrated in Fig. 2(b). From this figure, it can be noticed that both η_{rad}- and $P_{\text{rad}}/P_{\text{near}}$-optimized weights performed clearly the best and the FoM with TARC-optimized weights is the lowest in the entire frequency band. FoM with η_{rad} and $P_{\text{rad}}/P_{\text{near}}$ feeding weights is in average about 50% higher than that of η_{tot} or equal feeding weights. Only, at a single frequency (2.85 GHz) η_{tot} weights achieves equally good FoM as η_{rad} and $P_{\text{rad}}/P_{\text{near}}$ weights.

The improvement in FoM can be analyzed by studying separately total efficiency and SAR. As Fig. 3(a) shows, the differences in total efficiency obtained with different feeding weights are rather small, except in the TARC optimal weights which lead to significantly lower efficiency than others. Fig. 3(b) represents the 1-g maximum SAR when input power is 22.4 dBm (175 mW). Defining the input weights so that TARC is optimized produces clearly the highest SAR, almost
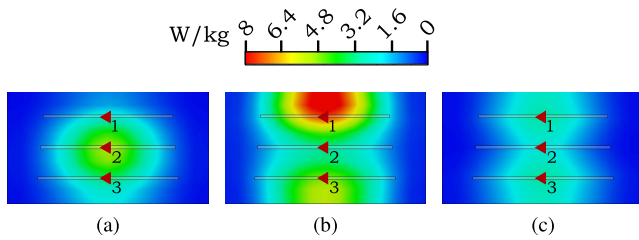
Fig. 4.   1-g SAR patterns of the three dipoles at 2.8 GHz with P_{in} = 22.4 dBm. (a) Equal, (b) TARC, and (c) P_{rad}/P_{near} input weights. The feeding ports, 1, 2, and 3 are marked with red arrows.

three times as high as with η_{rad} and P_{rad}/P_{near} weights. Also equal and η_{tot} weights produce about 30%–80% higher SAR than η_{rad} and P_{rad}/P_{near} weights.

SAR with both TARC and η_{tot} input weights varies rather much as a function of frequency, while the other optimization methods achieve less frequency-variant SAR. Both the high SAR and its frequency-dependent behavior can be explained with SAR patterns shown in Fig. 4. A high SAR value is obtained when the SAR maximum is concentrated on a small area as shown in Fig. 4(b) with TARC weights. Equal feeding achieves lower SAR than TARC-optimized weights since its SAR has distributed on a wider area near the center dipole. Accordingly, the SAR of both η_{rad} and P_{rad}/P_{near} weights obtain the lowest values since their patterns do not exhibit hot spots, like TARC, but spread more constantly as shown in Fig. 4(c). An SAR pattern with η_{tot} weights behaves similarly to the one of TARC weight except for around 2.85 GHz, where it obtains a local minimum. Around that local minimum, the SAR distribution is similar as with η_{rad} and P_{rad}/P_{near} weights.

Fig. 5 shows the amplitudes and phases of the TARC-, P_{rad}/P_{near}-, η_{rad}-, and η_{tot}-optimized input weights. The input weights obtained with P_{rad}/P_{near} and η_{rad} optimization goals are similar especially in the middle of considered frequency band. Therefore, their FoM and other results are similar. Clearly, P_{rad}/P_{near} weights have only moderate frequency dependence, while TARC and η_{tot} weights are strongly frequency-dependent. Since the radiation properties of an antenna cluster are not unique, different feeding weights can give the same far-field result. This also explains why at 2.85 GHz the results with η_{tot}, η_{rad}, and P_{rad}/P_{near} input weights are almost identical.

B. Metal-Rimmed Mobile Antenna Design

As a more realistic antenna design, we consider a metal-rimmed handset antenna held in a human hand as shown in Fig. 6. The overall dimensions of the device are 71 mm × 150 mm × 5 mm and the ground clearance is 3 mm all around the device. The minimum distance between the rim and the hand is 1 mm. We compare two antenna designs. In the first one, a 30 mm long element is placed on the rim (port 2 in Fig. 6). In the second one, we have a "three-element stack" of equal length 30 mm elements (ports 1, 2, and 3 in Fig. 6). The elements are overlapping so that element 2 locates on the rim (3 mm from the ground plane), and elements 3 and 1 are at the distance of 1 and 2 mm from the rim, respectively. The excitation for element 2 is located at the center of the element, element 1 is excited from the right end, and element 3 from the left end. The heights of elements 1 and 3 are 4 mm and the height of element 2 is 5 mm. The equal length of the elements enables a compact design, and the asymmetrical location of the feeding ports is favorable for the cluster design.

The same feeding weight optimization methods are used as in the case of three dipoles: TARC, η_{rad}, η_{tot}, and P_{rad}/P_{near}. The
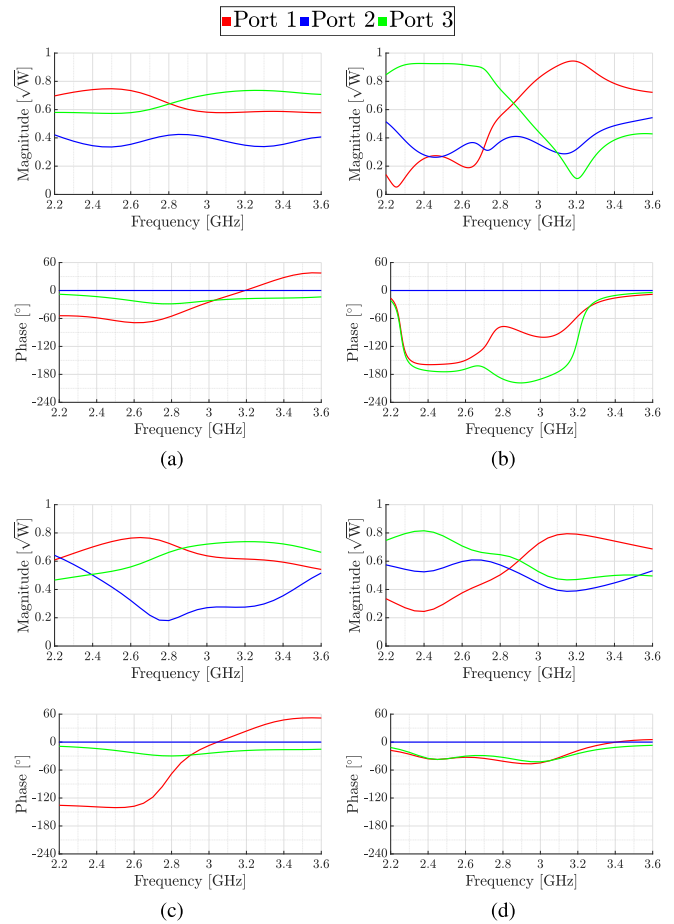

Fig. 5.   Magnitude (top) and phase (bottom) of (a) P_{rad}/P_{near}, (b) TARC, (c) η_{rad}, and (d) η_{tot} optimized input weights for the three dipoles.
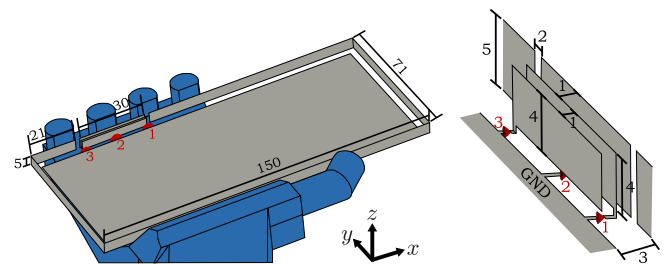

Fig. 6.   Mobile antenna with a metal rim and three feeding elements. The hand model is adopted from [29].

optimization results are compared with the nonoptimized case (equal) and with the one-element case (1-element).

Fig. 7 shows TARC and total efficiency for the metal-rimmed antenna with different optimization methods. The 5G frequency band n77 (3.3–4.2 GHz) has been marked with a black dashed line in the figure. Similar behavior as in the case of three dipoles can be noticed, and all optimization methods obtain adequate matching and total efficiency in the n77 band.

Similarly, as in the 3-dipole case, a clear advantage of multiport feeding with properly optimized weights, either P_{rad}/P_{near} or η_{rad} case, can be seen in the maximum SAR shown in Fig. 8. In the considered frequency band, the maximum SAR of the 1-port design is two to four times higher than that of the best three-port case. We may also observe that the choice of the optimization goal has a
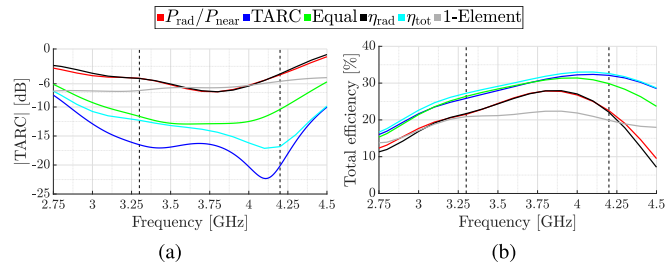
Fig. 7. (a) TARC and (b) total efficiency of the metal-rimmed mobile antenna with various feeding weights. 1-element stands for the single-element antenna design. The n77 band is marked with a black dashed line.
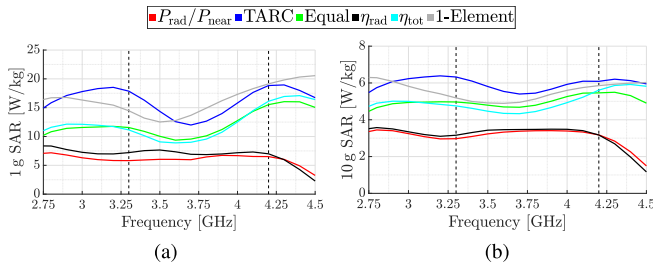

Fig. 8. (a) Maximum 1-g SAR and (b) maximum 10-g SAR of the mobile antenna with various feeding weights. The n77 band is marked with a black dashed line. The input power is 22.4 dBm (175 mW).
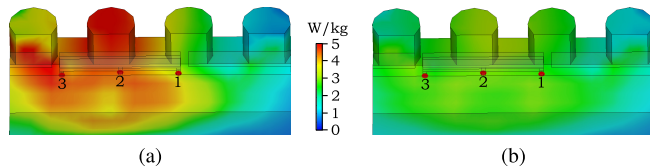

Fig. 9. 10-g SAR patterns of the metal-rimmed mobile antenna at 3.7 GHz with $P_{in} = 22.4$ dBm. (a) TARC and (b) P_{rad}/P_{near} optimal inputs.
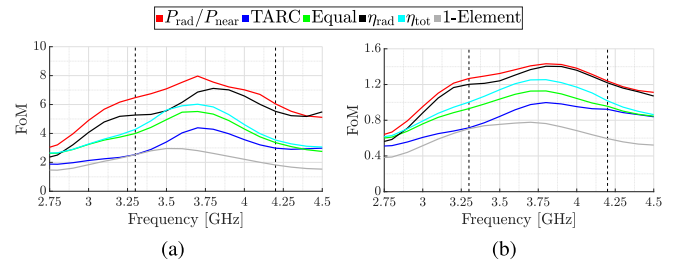

Fig. 10. FoM of the metal-rimmed mobile antenna calculated with (a) 1-g SAR and (b) with 10-g SAR. The n77 band is marked with a black dashed line.
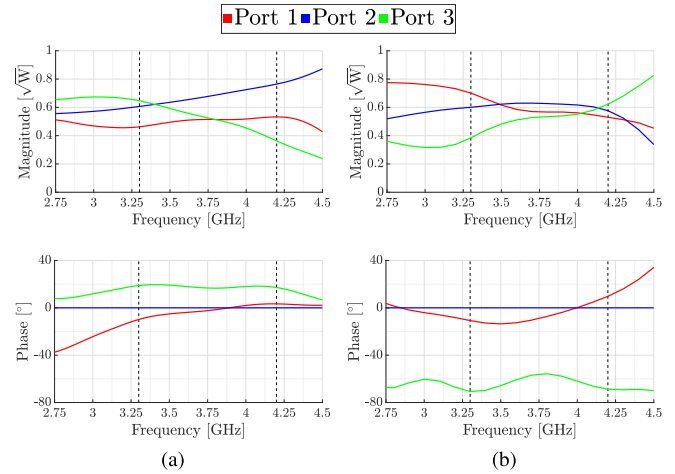

Fig. 11. Magnitude (top) and phase (bottom) of (a) TARC and (b) P_{rad}/P_{near}-optimized input weights for the metal-rimmed antenna. The n77 band is marked with a black dashed line.
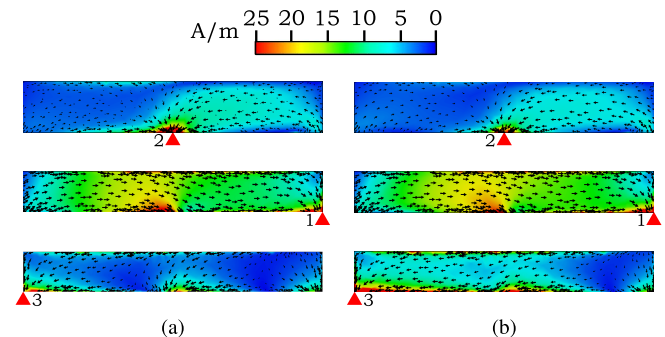

Fig. 12. Real part of the surface currents on the feeding elements of the metal-rimmed mobile antenna with (a) TARC and (b) P_{rad}/P_{near} input weights at 3.7 GHz. Locations of the discrete ports are marked with red arrows.

significant effect on the results. For example, optimizing the TARC of the 3-port design can lead to an even higher SAR than that in the 1-port design. In addition, the relative differences between the results of the optimization goals are larger in the case of 1-g SAR than in the case of 10-g SAR. SAR for a limb is defined for a 10-g tissue volume [1], [2] but we also show 1-g SAR for comparison. Obviously, in 1-g SAR, the tissue volumes are much smaller, since the maximum SAR values are significantly higher and more focused on the surface of the body than for 10-g SAR.

The SAR patterns with TARC and P_{rad}/P_{near} weights are shown in Fig. 9. Similar behavior as in the case of three dipoles can be observed. The SAR pattern with TARC weights has clearly stronger local maxima than with P_{rad}/P_{near} weights. Actually, one element and all other considered feeding methods, except P_{rad}/P_{near} and η_{rad}, show similar high local maxima as TARC weights. Hence, P_{rad}/P_{near} and η_{rad} weights lead to clearly the lowest SAR values.

Fig. 10 shows the FoM with various input weights. In computing FoM, both 1-g and 10-g maximum SAR are used. The results demonstrate that defining the input weights, so that the far-near field power ratio is maximized, leads to the best efficiency-SAR ratio on a wide frequency range.

To get more insights into the function of the multiport antenna feeding design with different optimization goals in SAR reduction, we next study both the input weights and the surface currents. Fig. 11 shows the amplitudes and phases of the P_{rad}/P_{near} and the TARC-optimized input weights. These results show that on the

n77 band, the input weights of both methods are near constants, and their amplitudes are almost equal. The main difference appears in the phase difference of the feeding signal of port 3 compared to the other ports. In the P_{rad}/P_{near} weights, this difference is about $-60°$, while in the TARC weights, it is about $+20°$.

In Fig. 12, we display the real part of the surface current on the antenna elements calculated with TARC and P_{rad}/P_{near} input weights at 3.7 GHz. The currents on the two outermost elements, elements 1 and 2, are akin due to similar amplitude and phase, while significant differences in the currents on element 3 can be observed. Since with P_{rad}/P_{near} weights, the currents on the element furthest from the hand (element 3) are stronger and the currents on the nearest element
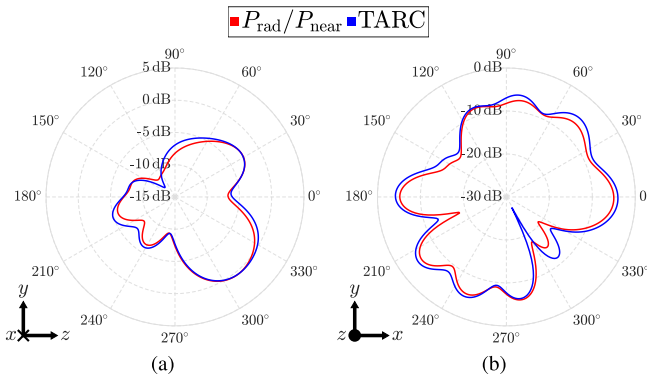
Fig. 13.   Realized gain of the metal-rimmed mobile antenna with TARC and $P_{\mathrm{rad}}/P_{\mathrm{near}}$ input weights at 3.7 GHz. (a) yz and (b) xy planes.

(element 2) are smaller than with TARC weights, SAR is lower with $P_{\mathrm{rad}}/P_{\mathrm{near}}$ input weights.

Fig. 13 illustrates the realized gain in xy and yz planes with TARC and $P_{\mathrm{rad}}/P_{\mathrm{near}}$ input weights at 3.7 GHz. Clearly, these patterns are nearly identical and thus the antenna radiation pattern is almost independent of the used input weights. This result further verifies that with the proposed method low SAR values can be obtained without sacrificing antenna radiation.

IV. Conclusion

A novel antenna design method based on the multiport cluster technique that simultaneously provides high efficiency and low SAR is introduced. The optimal weights of the feeding ports are found as a solution to a generalized eigenvalue problem expressed with the radiated and near-field power port matrices of the antenna. The feasibility of the proposed approach is demonstrated with a metal-rimmed mobile antenna held in the user's hand. More than 50% reduction in maximum SAR values can be obtained compared to a conventional single-port antenna design, without significantly sacrificing the efficiency. It is also shown that solely maximizing matching (minimizing TARC) can lead to prohibitively high SAR values.

References

[1] R. E. Fields, "Evaluating compliance with FCC guidelines for human exposure to radiofrequency electromagnetic fields," *OET Bull.*, vol. 65, no. 10, pp. 1–65, 1997.

[2] *IEEE Standard for Safety Levels With Respect to Human Exposure to Electric, Magnetic, and Electromagnetic Fields, 0 Hz to 300 GHz*, Standard IEEE Std C95.1-2019, Oct. 2019.

[3] H. H. Zhang, G. G. Yu, Y. Liu, Y. X. Fang, G. Shi, and S. Wang, "Design of low-SAR mobile phone antenna: Theory and applications," *IEEE Trans. Antennas Propag.*, vol. 69, no. 2, pp. 698–707, Feb. 2021.

[4] B. Lu, B. Pang, W. Hu, and W. Jiang, "Low-SAR antenna design and implementation for mobile phone applications," *IEEE Access*, vol. 9, pp. 96444–96452, 2021.

[5] H. H. Zhang *et al.*, "Low-SAR MIMO antenna array design using characteristic modes for 5G mobile phones," *IEEE Trans. Antennas Propag.*, vol. 70, no. 4, pp. 3052–3057, Apr. 2022.

[6] H. H. Zhang, X. Z. Liu, G. S. Cheng, Y. Liu, G. M. Shi, and K. Li, "Low-SAR four-antenna MIMO array for 5G mobile phones based on the theory of characteristic modes of composite PEC-lossy dielectric structures," *IEEE Trans. Antennas Propag.*, vol. 70, no. 3, pp. 1623–1631, Mar. 2022.

[7] C. T. Liao, Z. K. Yang, and H. M. Chen, "Multiple integrated antennas for wearable fifth-generation communication and Internet of Things applications," *IEEE Access*, vol. 9, pp. 120328–120346, 2021.

[8] T. Le and T.-Y. Yun, "Wearable dual-band high-gain low-SAR antenna for off-body communication," *IEEE Antennas Wireless Propag. Lett.*, vol. 20, no. 7, pp. 1175–1179, Jul. 2021.

[9] M. El Atrash, M. A. Abdalla, and H. M. Elhennawy, "A wearable dual-band low profile high gain low SAR antenna AMC-backed for WBAN applications," *IEEE Trans. Antennas Propag.*, vol. 67, no. 10, pp. 6378–6388, Oct. 2019.

[10] P. Bernardi, M. Cavagnaro, S. Pisa, and E. Piuzzi, "Specific absorption rate and temperature increases in the head of a cellular-phone user," *IEEE Trans. Microw. Theory Techn.*, vol. 48, no. 7, pp. 1118–1126, Jul. 2000.

[11] A. Hadjem, D. Lautru, C. Dale, M. F. Wong, V. F. Hanna, and J. Wiart, "Study of specific absorption rate (SAR) induced in two child head models and in adult heads using mobile phones," *IEEE Trans. Microw. Theory Techn.*, vol. 53, no. 1, pp. 4–11, Jan. 2005.

[12] S. S. Zhekov, A. Tatomirescu, E. Foroozanfard, and G. F. Pedersen, "Experimental investigation on the effect of user's hand proximity on a compact ultrawideband MIMO antenna array," *IET Microw., Antennas Propag.*, vol. 10, no. 13, pp. 1402–1410, 2016.

[13] M. I. Kitra, C. J. Panagamuwa, P. McEvoy, J. C. Vardaxoglou, and J. R. James, "Low SAR ferrite handset antenna design," *IEEE Trans. Antennas Propag.*, vol. 55, no. 4, pp. 1155–1164, Apr. 2007.

[14] K. H. Chan, K. M. Chow, L. C. Fung, and S. W. Leung, "Effects of using conductive materials for SAR reduction in mobile phones," *Microw. Opt. Technol. Lett.*, vol. 44, no. 2, pp. 140–144, Jan. 2005, doi: 10.1002/MOP.20569.

[15] A. Hirata, T. Adachi, and T. Shiozawa, "Folded-loop antenna with a reflector for mobile handsets at 2.0 GHz," *Microw. Opt. Technol. Lett.*, vol. 40, no. 4, pp. 272–275, 2004, doi: 10.1002/MOP.11350.

[16] M. T. Islam, N. Misran, T. S. Ling, and M. R. I. Faruque, "Reduction of specific absorption rate (SAR) in the human head with materials and metamaterial," in *Proc. Int. Conf. Electr. Eng. Informat.*, vol. 2, Aug. 2009, pp. 707–710.

[17] R. Ikeuchi and A. Hirata, "Dipole antenna above EBG substrate for local SAR reduction," *IEEE Antennas Wireless Propag. Lett.*, vol. 10, pp. 904–906, 2011.

[18] J.-N. Hwang and F.-C. Chen, "Reduction of the peak SAR in the human head with metamaterials," *IEEE Trans. Antennas Propag.*, vol. 54, no. 12, pp. 3763–3770, Dec. 2006.

[19] R. Das and H. Yoo, "Application of a compact electromagnetic bandgap array in a phone case for suppression of mobile phone radiation exposure," *IEEE Trans. Microw. Theory Techn.*, vol. 66, no. 5, pp. 2363–2372, May 2018.

[20] C. Volmer, J. Weber, R. Stephan, K. Blau, and M. A. Hein, "An eigenanalysis of compact antenna arrays and its application to port decoupling," *IEEE Trans. Antennas Propag.*, vol. 56, no. 2, pp. 360–370, Feb. 2008.

[21] J.-M. Hannula, J. Holopainen, and V. Viikari, "Concept for frequency-reconfigurable antenna based on distributed transceivers," *IEEE Antennas Wireless Propag. Lett.*, vol. 16, pp. 764–767, 2017.

[22] R. Kormilainen, J.-M. Hannula, T. O. Saarinen, A. Lehtovuori, and V. Viikari, "Realizing optimal current distributions for radiation efficiency in practical antennas," *IEEE Antennas Wireless Propag. Lett.*, vol. 19, no. 5, pp. 731–735, May 2020.

[23] Z. Zhang, *Antenna Design for Mobile Devices*, 2nd ed. Singapore: Wiley, 2017.

[24] B. Xu, M. Gustafsson, S. Shi, K. Zhao, Z. Ying, and S. He, "Radio frequency exposure compliance of multiple antennas for cellular equipment based on semidefinite relaxation," *IEEE Trans. Electromagn. Compat.*, vol. 61, no. 2, pp. 327–336, Apr. 2019.

[25] *IEC/IEEE International Standard—Determining the Peak Spatial-Average Specific Absorption Rate (SAR) in the Human Body From Wireless Communications Devices, 30 MHz to 6 GHz—Part 1: General Requirements for Using the Finite-Difference Time-Domain (FDTD) Method for SAR Calculations*, Standard IEC/IEEE 62704-1:2017, Oct. 2017.

[26] A. Stjernman, "Relationship between radiation patter correlation and scattering matrix of lossless and lossy antennas," *Electron. Lett.*, vol. 41, no. 12, pp. 678–680, Jun. 2005.

[27] P. Ylä-Oijala, M. Taskinen, and J. Sarvas, "Surface integral equation method for general composite metallic and dielectric structures with junctions," *Prog. Electromagn. Res.*, vol. 52, pp. 81–108, 2005.

[28] P. Ylä-Oijala and M. Taskinen, "Calculation of CFIE impedance matrix elements with RWG and $n \times$ RWG functions," *IEEE Trans. Antennas Propag.*, vol. 51, no. 8, pp. 1837–1846, Aug. 2003.

[29] R. Luomaniemi, P. Yla-Oijala, A. Lehtovuori, and V. Viikari, "Designing hand-immune handset antennas with adaptive excitation and characteristic modes," *IEEE Trans. Antennas Propag.*, vol. 69, no. 7, pp. 3829–3839, Jul. 2021.